Available online at www.sciencedirect.com
ScienceDirect
Journal of Solid State Chemistry 180 (2007) 1020–1027
JOURNAL OF SOLID STATE CHEMISTRY
www.elsevier.com/locate/jssc

Single-crystal synthesis, structure analysis, and physical properties of the calcium ferrite-type $Na_xTi_2O_4$ with $0.558 < x < 1$

Yasuhiko Takahashi[a], Kunimitsu Kataoka[a,b], Ken-ichi Ohshima[b], Norihito Kijima[a], Junji Awaka[a], Kenji Kawaguchi[a], Junji Akimoto[a,*]

[a]*National Institute of Advanced Industrial Science and Technology (AIST), 1-1-1 Higashi, Tsukuba 305-8565, Japan*
[b]*Institute of Materials Science, University of Tsukuba, Tsukuba 305-8573, Japan*

Received 11 October 2006; received in revised form 10 December 2006; accepted 24 December 2006
Available online 5 January 2007

Abstract

Single crystals of calcium ferrite $CaFe_2O_4$-type $NaTi_2O_4$ having millimeter-sized needle shapes were synthesized by a reaction of Na metal and TiO_2 in a sealed iron vessel at 1473 K. Sodium-deficient $Na_xTi_2O_4$ single crystals with $0.558 < x < 1$ were successfully synthesized by a topotactic oxidation reaction using $NaTi_2O_4$ single crystals as parent materials. The crystal structures of $Na_xTi_2O_4$ with $x = 0.970$, 0.912, 0.799, 0.751, 0.717, 0.686, 0.611, and 0.558 were determined by the single-crystal X-ray diffraction method. The basic framework constructed by the $Ti1O_6$ and $Ti2O_6$ double rutile chains was maintained in these $Na_xTi_2O_4$ compounds. Based on the results of bond valence analysis, we speculated that the Ti1 sites are preferentially occupied by Ti^{3+} cations over the compositional range of $0.8 < x < 1$, while both the Ti1 and Ti2 sites are randomly occupied by Ti^{3+} and Ti^{4+} cations at $x = 0.558$. Magnetic susceptibility data indicated that the broad maximum around 40 K observed in as-grown $NaTi_2O_4$ is suppressed by an Na deficiency and vanishes in $Na_{0.717}Ti_2O_4$. The electrical resistivity increased with the Na deficiency; however, it was still semiconductive in $Na_{0.799}Ti_2O_4$.

Keywords: $NaTi_2O_4$; Crystal growth; Topotactic oxidation; Na deficiency; Structure analysis

1. Introduction

The mixed-valence ternary oxides of Ti^{3+}/Ti^{4+} display a wide range of interesting chemical, electronic, and magnetic properties; for example, spinel-type lithium titanate compounds $Li_{1+x}Ti_{2-x}O_4$ with $0 \leqslant x < 1/3$ exhibit superconductivity below $T_c = 13$ K [1], and the end member compound $Li_{4/3}Ti_{5/3}O_4$ ($x = 1/3$) is attractive for use as a negative electrode material in advanced lithium-ion batteries [2]. Furthermore, metallic perovskite-type titanates such as $Sr_{1-x}La_xTiO_3$ have recently been investigated as potential candidates for use as *n*-type thermoelectric materials [3].

$NaTi_2O_4$ has the orthorhombic calcium ferrite $CaFe_2O_4$-type structure [4]. The average Ti valence state in $NaTi_2O_4$ is +3.5, that is, there are equal numbers of Ti^{3+} ($3d^1$) and Ti^{4+} ($3d^0$) cations in the structure. Therefore, $NaTi_2O_4$ should exhibit interesting chemical and physical properties such as superconductivity in spinel-type $LiTi_2O_4$ [1,5] and lithium deintercalation–intercalation reactions in ramsdellite-type $Li_{0.5}TiO_2$ [6–9].

In the synthesis of $NaTi_2O_4$ at high temperatures, both the Ti lower-valence state (Ti^{3+}) and the Na vapor pressure should be maintained in order to suppress the decomposition reaction:

$$Na_2O + Ti_2O_3 \rightarrow 2Na \uparrow + 2TiO_2.$$

Previous studies [10,11] have shown that a closed system—particularly one that employs a redox reaction of Na metal and TiO_2—is useful for synthesizing single crystals of reduced sodium titanates at 1473–1673 K. On the other hand, Geselbracht et al. [12] have recently reported a new synthetic route for obtaining $NaTi_2O_4$ using a reduction reaction of $Na_8Ti_5O_{14}$ with Ti metal in a molten NaCl/KCl salt flux at 1043 K. This method provides an easy means to produce small needle-shaped $NaTi_2O_4$ samples

*Corresponding author. Fax: +81 29 861 9214.
E-mail address: j.akimoto@aist.go.jp (J. Akimoto).

0022-4596/$ - see front matter © 2007 Elsevier Inc. All rights reserved.
doi:10.1016/j.jssc.2006.12.023

at a relatively low temperature. More recently, the electrical and magnetic properties of this compound have been measured for the first time by using such samples [13].

The basic unit of the $NaTi_2O_4$ structure is the "double rutile" chain, in which a pair of edge-sharing TiO_6 octahedra piles up along the *c*-axis with sharing edges. Four chains are linked by the sharing of vertices to form a framework structure and produce one-dimensional tunnels containing Na cations [4,13]. There are two Ti sites in this structure, which are reported to be randomly occupied by Ti^{3+} and Ti^{4+} based on similar average Ti–O bond distances [4]. On the other hand, the partial charge segregation of electron density into one of the two Ti sites has been recently suggested from the results of band calculations and transport measurements [13].

In the present study, we report the single-crystal synthesis of Na-deficient $Na_xTi_2O_4$ with Na content x over the range of $0.558 < x < 1$ by a topotactic oxidation reaction using single crystals of $NaTi_2O_4$ as parent materials. The crystal structures and some of the physical properties of $Na_xTi_2O_4$ with different x values have been revealed for the first time. We propose a compositional charge order–disorder transition around $x = 0.8$ for $Na_xTi_2O_4$.

2. Experimental procedures

2.1. Single-crystal synthesis

Single crystals of $NaTi_2O_4$ were synthesized by the reaction of Na metal and TiO_2 at 1473 K. TiO_2 powder (99.9%) was used after firing at 673 K for several hours in air. Sodium metal (99%), which is sold in stick form, was cut into the desired quantities in a glove box filled with argon gas. They were introduced at a nominal molar ratio of Na:Ti = 1.1:2 into an iron vessel (inner volume of ca. 10 cm^3) in the glove box. After the vessel was closed by screwing the top with a vise, it was heated in a resistance furnace at 1473 K with argon gas flow for several hours and then slowly cooled to room temperature at a rate of 3 K/h. In many cases, no apparent leakage of Na vapor was observed from the vessel. After cooling, the vessel was opened in air with a saw.

Black, needle-shaped $NaTi_2O_4$ single crystals with dimensions of approximately $3.0 \times 0.3 \times 0.3\,mm^3$ (maximum) were obtained, as shown in Fig. 1. The crystals thus obtained were investigated by scanning electron microscopy–energy-dispersive X-ray analysis (SEM-EDX; JEOL JSM-5400). The chemical composition of the as-grown crystals was determined to be Na:Ti = 1:2 by the EDX analysis. No iron from the reaction vessel was detected in the chemical analysis.

We noted that the $NaTi_2O_4$ crystals always synthesized together with the colorless $Na_8Ti_5O_{14}$ crystals at the bottom of the vessel. In addition, small needle-shaped $Na_8Ti_5O_{14}$ crystals ($10 \times 10 \times 1\,\mu m^3$) were found in the surface regions of the large needle crystals of $NaTi_2O_4$. Interestingly, $NaTi_2O_4$ had been recently synthesized using a reduction reaction of $Na_8Ti_5O_{14}$ by Ti metal powder in a NaCl/KCl molten salt at 1043 K [12]. These facts may suggest that the formation of $Na_8Ti_5O_{14}$ crystals plays an important role in the crystal growth of $NaTi_2O_4$ in the present study.

Fig. 1. As-grown needle-shaped $NaTi_2O_4$ single crystals (1 grid = 1 mm).

The as-grown $NaTi_2O_4$ crystals remain stable in air for a few months. However, an Na site deficiency was observed in the crystals kept in air for more than several months, together with the deposition of Na_2CO_3 powder on the crystal surfaces. Therefore, we kept the crystals under a vacuum or in argon-filled desiccators.

2.2. Topotactic oxidation

Sodium-deficient $Na_xTi_2O_4$ single crystals were prepared by a topotactic chemical oxidation method using an acidic solution. In previous studies, this oxidation method had been successfully applied for the syntheses of hollandite-type K_xTiO_2 [14] and ramsdellite-type Li_xTiO_2 [7–9]. The selected $NaTi_2O_4$ single crystals with typical dimensions of $0.2 \times 0.1 \times 0.1\,mm^3$ were soaked in a 1 M HCl solution at room temperature for an appropriate number of days. No stirring or heating was performed. The bubbling of H_2 gas from the surface regions of the crystals was observed, which suggested the production of the Na-deficient single crystals by the reaction:

$$2NaTi_2O_4 + 2\delta H^+ \rightarrow 2Na_{1-\delta}Ti_2O_4 + 2\delta Na^+ + \delta H_2 \uparrow .$$

By employing soaking times ranging from a few days to several months, we succeeded in preparing eight Na-deficient single-crystal specimens having chemical compositions of $x = 0.970$, 0.912, 0.799, 0.751, 0.717, 0.686, 0.611, and 0.558 in $Na_xTi_2O_4$. In the present study, the oxidation reaction could not be fully completed, and the most oxidized specimen had a chemical composition of $Na_{0.558}Ti_2O_4$. The chemical formulae of these oxidized crystals were determined by the present single-crystal X-ray structure analyses. The values showed good consistency

with the analytical data obtained by SEM-EDX using single-crystal specimens.

2.3. Single-crystal X-ray diffraction

Eight small crystals of $Na_xTi_2O_4$ having different Na contents were mounted on glass fibers for performing single-crystal X-ray diffraction studies. The crystals were examined with an X-ray precession camera (Mo$K\alpha$ radiation) to check the crystal quality and to determine the lattice parameters, systematic extinctions, and possible superstructures. Precession photographs of these $Na_xTi_2O_4$ single crystals indicate that all the Na-deficient compounds belong to the orthorhombic system with the possible space group *Pnam* or $Pna2_1$, which remains unchanged from that of the parent $NaTi_2O_4$ crystal [4]. Fig. 2 shows the $\{hk0\}^*$ and $\{h0l\}^*$ precession photographs of $Na_{0.558}Ti_2O_4$, taken at room temperature. No additional spots indicating ordered structure and diffuse scattering could be observed in these photographs.

Single-crystal intensity data of the Na-deficient samples were collected in the $2\theta-\omega$ scan mode at a scan rate of 4°/min at 300 K on a Rigaku AFC-5S four-circle diffractometer (operating conditions: 40 kV, 30 mA) using graphite-monochromatized Mo$K\alpha$ radiation ($\lambda = 0.71073$ Å); then, they were reduced to structure factors after due corrections for absorption and Lorentz and polarization effects. The fluctuations in the intensities were monitored by examining a set of three standard reflections ((600), (080), and (002)) which were taken after every 50 measurements.

Structure refinements were carried out with the atomic coordinates of $NaTi_2O_4$ using the *Pnam* space group [4]. The Na site occupancy values were refined in the calculations. The converged final R and wR values and other experimental and crystallographic data are summarized in Table 1. The final atomic coordinates and displacement parameters are given in Table 2. All calculations were carried out using the Xtal3.5 package program [15].

2.4. Physical measurements

Electrical resistivities of the $Na_xTi_2O_4$ single-crystal samples with $x = 1$ and 0.799 were measured between 100 and 300 K by a conventional direct-current four-probe method using spring-type gold leads. The single-crystal samples measured were needle-shaped with lengths of approximately 1 mm. Ohmic contacts were confirmed by a linear V–I characteristic at 100 and 300 K. The thermoelectric power of the $Na_xTi_2O_4$ ($x = 0.717$) crystals was measured at 300 K with a comparative technique using a constantan standard in a Seebeck measurement system (MMR Technologies, Inc., SB-100). Magnetic susceptibilities of three $Na_xTi_2O_4$ samples with $x = 1$, 0.912, and 0.717 were measured as a function of temperature by using a SQUID magnetometer (Quantum Design, MPMS). The

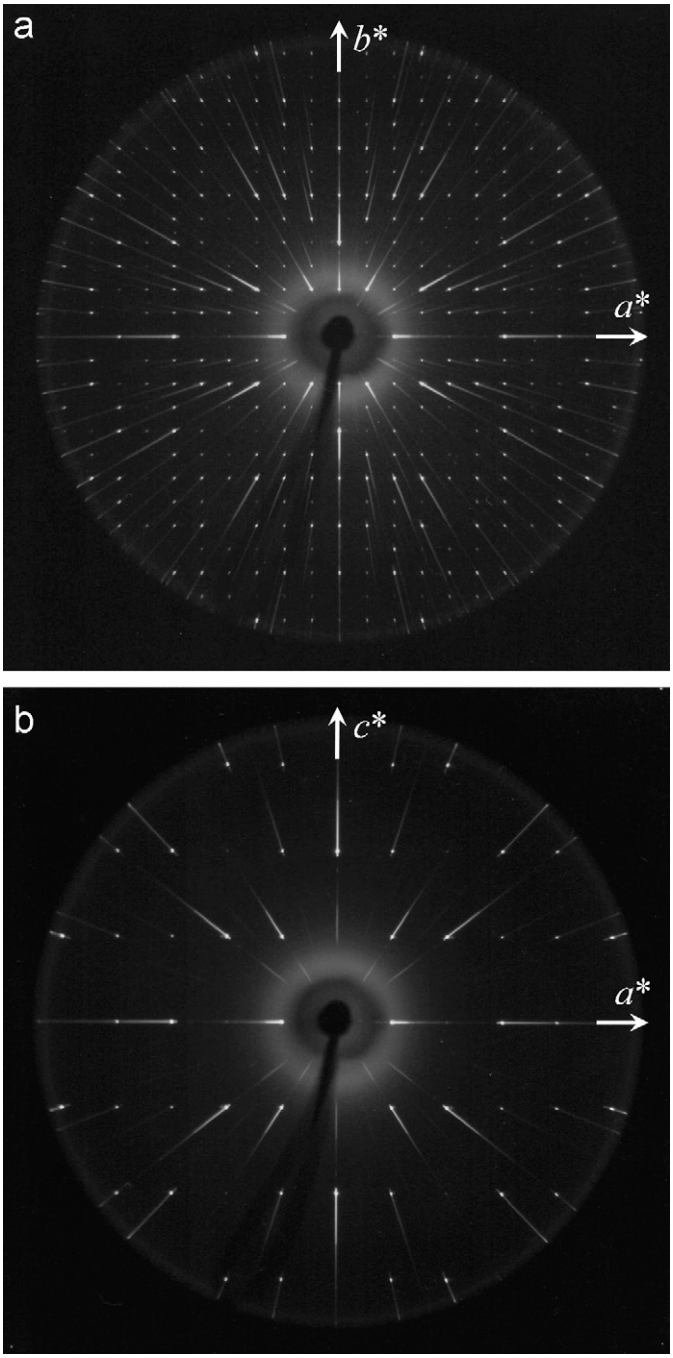

Fig. 2. (a) $\{hk0\}^*$ and (b) $\{h0l\}^*$ precession photographs of $Na_{0.558}Ti_2O_4$. Mo$K\alpha$ radiation filtered by a Zr foil was used.

measurements were carried out under field cooling at 10 kOe between 4 and 300 K. Diamagnetic corrections for the magnetic susceptibilities were taken into account. Because the single-crystal size was relatively small, the magnetic measurements were performed on a batch of randomly oriented single crystals of $Na_xTi_2O_4$. We measured the X-ray powder diffraction data using the single-crystal samples before the magnetic measurements. Because the samples were washed with ethanol and the $Na_8Ti_5O_{14}$ crystals were carefully excluded, no impurity phases were observed in the XRD patterns.

Table 1
Experimental and crystallographic data for $Na_xTi_2O_4$

Na content x	0.970(3)	0.912(3)	0.799(5)	0.751(4)	0.717(4)	0.686(3)	0.611(4)	0.558(3)
Crystal system	Orthorhombic	Orthorhombic	Orthorhombic	Orthorhombic	Orthorhombic	Orthorhombic	Orthorhombic	Orthorhombic
Space group	*Pnam*	*Pnam*	*Pnam*	*Pnam*	*Pnam*	*Pnam*	*Pnam*	*Pnam*
a (Å)	9.2618(7)	9.2609(7)	9.2467(12)	9.2113(8)	9.2005(10)	9.1900(11)	9.166(3)	9.139(2)
b (Å)	10.7541(7)	10.7537(7)	10.7481(11)	10.7467(7)	10.7451(10)	10.7423(10)	10.731(4)	10.719(4)
c (Å)	2.9548(5)	2.9550(5)	2.9535(8)	2.9502(5)	2.9505(7)	2.9521(7)	2.9533(8)	2.9560(7)
V (Å^3)	294.30(6)	294.29(6)	293.53(9)	292.04(6)	291.69(8)	291.44(8)	290.49(16)	289.57(14)
Z	4	4	4	4	4	4	4	4
D_x (g/cm^3)	4.109	4.079	4.030	4.026	4.013	4.000	3.974	3.959
Crystal size (μm)	150 × 150 × 100	180 × 100 × 40	100 × 100 × 70	190 × 100 × 60	180 × 80 × 70	150 × 100 × 100	150 × 150 × 100	220 × 80 × 20
Maximum 2θ (deg)	110	110	110	110	110	110	110	110
Transmission factors								
Min.	0.488	0.543	0.616	0.525	0.469	0.572	0.470	0.501
Max.	0.609	0.794	0.709	0.730	0.704	0.635	0.610	0.891
Independent reflections	2108	2108	2095	2095	2083	2088	2202	2190
Observed reflections ($>4\sigma$)	1726	1654	1335	1598	1683	1726	1638	1248
Number of variables	45	45	45	45	45	45	45	45
Extinction parameter g	364(15)	696(20)	122(16)	553(20)	275(13)	244(13)	419(15)	197(20)
R (%)	3.634	3.493	5.193	3.962	4.164	3.761	4.299	6.108
wR [w $= 1/\sigma^2 F$] (%)	3.138	3.107	4.156	3.591	3.145	3.101	3.613	4.791
Largest diff. peak and hole (e/Å^3)	2.408, −2.114	2.222, −2.336	5.728, −5.332	2.134, −3.743	2.226, −3.122	3.479, −3.496	3.746, −5.054	6.950, −8.079

Table 2
Atomic coordinates[a] and equivalent isotropic displacement parameters (Å^2) for $Na_xTi_2O_4$

Na content x		0.970(3)	0.912(3)	0.799(5)	0.751(4)	0.717(4)	0.686(3)	0.611(4)	0.558(3)
Na	x	0.24379(11)	0.24376(12)	0.2435(2)	0.24325(18)	0.24295(17)	0.24295(16)	0.2429(2)	0.2431(4)
	y	0.34721(9)	0.34701(10)	0.34664(19)	0.34628(15)	0.34565(13)	0.34613(13)	0.34578(16)	0.3459(3)
	U_{eq}	0.0102(4)	0.0111(3)	0.0117(9)	0.0187(5)	0.0199(5)	0.0215(5)	0.0192(9)	0.0181(16)
Ti1	x	0.06615(4)	0.06559(4)	0.06468(7)	0.06343(5)	0.06289(5)	0.06231(4)	0.06164(5)	0.06032(9)
	y	0.10974(3)	0.11012(3)	0.11120(6)	0.11163(4)	0.11198(4)	0.11234(3)	0.11292(4)	0.11370(7)
	U_{eq}	0.00629(6)	0.00689(7)	0.0086(2)	0.00748(8)	0.00952(8)	0.00998(7)	0.00946(14)	0.0126(3)
Ti2	x	0.08204(4)	0.08231(4)	0.08256(7)	0.08366(4)	0.08388(4)	0.08408(4)	0.08415(4)	0.08417(8)
	y	0.60462(3)	0.60444(3)	0.60384(6)	0.60360(4)	0.60349(3)	0.60323(3)	0.60301(3)	0.60279(7)
	U_{eq}	0.00589(6)	0.00616(6)	0.0074(2)	0.00573(7)	0.00737(7)	0.00753(6)	0.00670(11)	0.0092(2)
O1	x	0.28855(16)	0.28942(16)	0.2904(3)	0.29181(18)	0.29205(17)	0.29266(15)	0.29358(16)	0.2947(3)
	y	0.65118(13)	0.65027(14)	0.6484(2)	0.64737(16)	0.64766(14)	0.64618(13)	0.64612(14)	0.6451(3)
	U_{eq}	0.0078(3)	0.0081(3)	0.0088(9)	0.0070(3)	0.0088(3)	0.0088(3)	0.0082(5)	0.0099(10)
O2	x	0.38768(15)	0.38760(15)	0.3879(3)	0.38760(17)	0.38824(16)	0.38803(14)	0.38827(16)	0.3883(3)
	y	0.98034(13)	0.98066(13)	0.9809(2)	0.98186(15)	0.98173(13)	0.98206(12)	0.98239(13)	0.9818(3)
	U_{eq}	0.0062(3)	0.0066(3)	0.0075(9)	0.0051(3)	0.0066(3)	0.0068(2)	0.0060(4)	0.0083(9)
O3	x	0.47930(16)	0.47902(17)	0.4783(3)	0.4781(2)	0.47715(17)	0.47667(16)	0.47656(17)	0.4759(3)
	y	0.21750(13)	0.21741(13)	0.2171(2)	0.21674(15)	0.21676(13)	0.21646(12)	0.21672(13)	0.2170(3)
	U_{eq}	0.0072(3)	0.0075(3)	0.0086(9)	0.0065(3)	0.0081(3)	0.0083(3)	0.0073(5)	0.0101(10)
O4	x	0.07990(16)	0.07920(16)	0.0783(3)	0.07766(18)	0.07710(17)	0.07700(15)	0.07625(16)	0.0761(3)
	y	0.92999(13)	0.92995(13)	0.9296(2)	0.92997(15)	0.92972(13)	0.92957(12)	0.92935(13)	0.9288(3)
	U_{eq}	0.0069(3)	0.0070(3)	0.0082(9)	0.0056(3)	0.0072(3)	0.0075(3)	0.0062(4)	0.0079(9)

[a]All atoms in point position 4c, $\pm(x, y, 1/4)$, $\pm(1/2-x, 1/2+y, 3/4)$.

3. Results and discussion

3.1. Lattice parameters

Table 1 lists the lattice parameters of the $Na_xTi_2O_4$ compounds with $0.558 < x < 1$, determined by least-squares refinement using 2θ values of 25 strong reflections over the range 50–70° and Mo$K\alpha_1$ ($\lambda = 0.70926$ Å) on the four-circle diffractometer. Fig. 3 shows the relationship between the lattice parameters and x in the $Na_xTi_2O_4$ samples. Both the a- and b-axis lengths decrease with x, while the c-axis length shows a minimum value at $x = 0.751$. Furthermore, the a-axis length and the unit-cell volume V show a discontinuity between $x = 0.751$ and 0.799. These facts

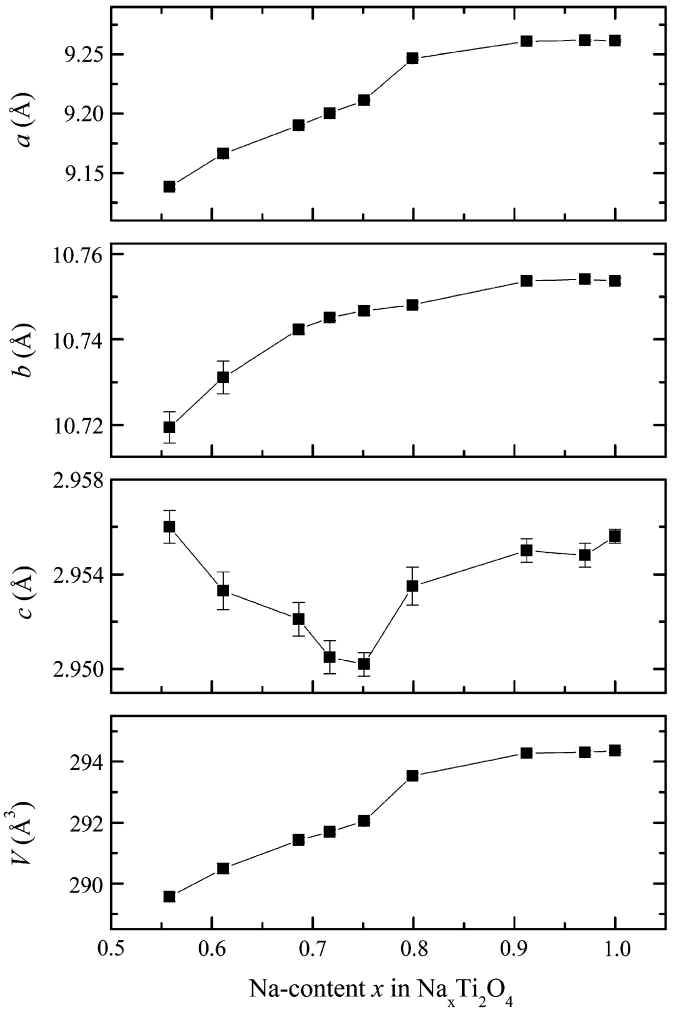

Fig. 3. Lattice parameters versus Na content x in the $Na_xTi_2O_4$ compounds.

may suggest a structural change at this compositional range. However, the precession photographs taken at room temperature indicate that the average structure of $Na_{0.558}Ti_2O_4$ remains unchanged from the as-grown $NaTi_2O_4$ structure, as mentioned earlier (Fig. 2). The discontinuity of the lattice parameter change around $x = 0.75$ may be caused by the magnetic Ti^{3+}–Ti^{3+} spin correlation, as discussed later. From the result of the present Na deintercalation reactions, we conclude that the lattice volume in $Na_{0.558}Ti_2O_4$ is smaller than that in the parent $NaTi_2O_4$ crystal by 4.73 Å^3, which is 1.6% of the host unit-cell volume. A similar contraction in the lattice volume has been previously demonstrated in ramsdellite-type $Li_xTi_2O_4$ with $0<x<1$ [7].

3.2. Crystal structures

The projection of the crystal structure of $Na_xTi_2O_4$ with $x = 0.558$ along the c-axis direction is shown in Fig. 4. The selected bond distances of $Na_{0.970}Ti_2O_4$, $Na_{0.912}Ti_2O_4$, $Na_{0.799}Ti_2O_4$, $Na_{0.751}Ti_2O_4$, $Na_{0.717}Ti_2O_4$, $Na_{0.686}Ti_2O_4$, $Na_{0.616}Ti_2O_4$, and $Na_{0.558}Ti_2O_4$ are listed in Table 3, in

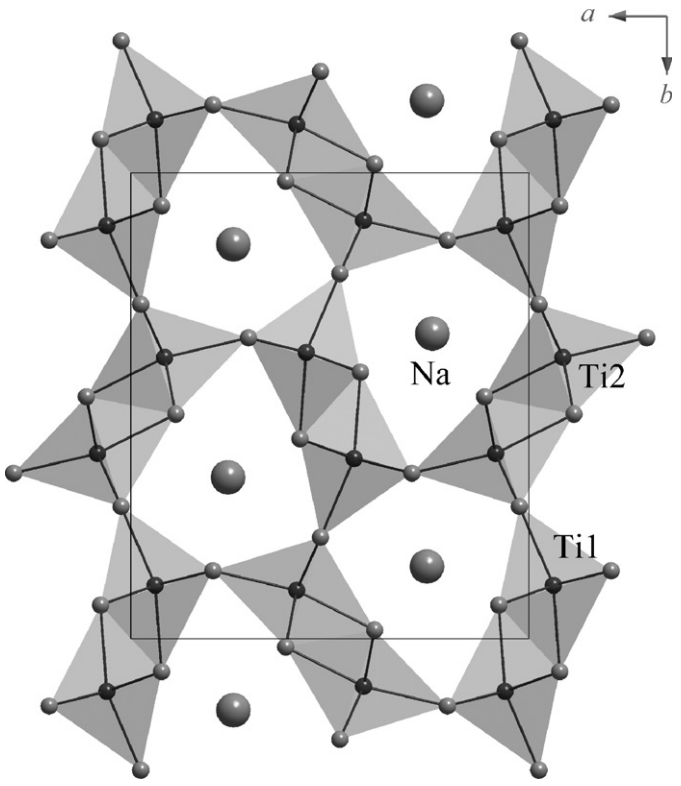

Fig. 4. Crystal structure of $Na_{0.558}Ti_2O_4$ viewed along [001]. TiO_6 are illustrated as octahedra, and the Na atoms appear as large balls.

comparison with the data of as-grown $NaTi_2O_4$ [4]. The basic framework of the TiO_6 double rutile chain is maintained in the $Na_xTi_2O_4$ compounds with $0.558<x<1$. Similar to the case of the parent $NaTi_2O_4$ crystal, the Na atom is surrounded by eight O atoms in a bicapped trigonal prism in these compounds. The mean Na–O distance increases, but very slightly, with the Na deficiency from 2.481 Å in $NaTi_2O_4$ to 2.489 Å in $Na_{0.558}Ti_2O_4$. This fact suggests the stability of the tunnel structure against the Na deintercalation reaction.

Both the Ti1 and Ti2 atoms are octahedrally coordinated by six O atoms in these compounds, as shown in Fig. 4. The Ti1–O distance varies over the short range of 1.972–2.013 Å in $Na_{0.558}Ti_2O_4$, in comparison with that of 1.932–2.051 Å in the parent $NaTi_2O_4$ compound (Fig. 5a). Note that the shortest Ti1–O4′ distance for the $Ti1O_6$ octahedron increases with the Na deficiency from 1.932 Å in $NaTi_2O_4$ to 1.988 Å in $Na_{0.558}Ti_2O_4$. Accordingly, the Ti1–O octahedral distortion value Δ decreases with the Na deficiency from 4.5×10^{-4} in $NaTi_2O_4$ to 0.6×10^{-4} in $Na_{0.558}Ti_2O_4$. Here, Δ is defined as being equal to $1/6\ \Sigma\{(R_i-R_m)/R_m\}^2$, where R_i and R_m denote the individual and average cation–oxygen distances, respectively, in an octahedron [16]. On the other hand, the Ti2–O octahedra show a Δ variation over a short range from 0.3×10^{-4} to 0.6×10^{-4} in these compounds. Considering the Ti–O bond distance, we can conclude that the $Ti1O_6$ octahedral distortion decreases with the Na deficiency in the $Na_xTi_2O_4$ compounds, and the coordination

Table 3
Selected bond distances (Å) for $Na_xTi_2O_4$

Na content x	1[a]	0.970(3)	0.912(3)	0.799(5)	0.751(4)	0.717(4)	0.686(3)	0.611(4)	0.558(3)
Na–O1 ×2	2.588(2)	2.592(2)	2.599(2)	2.611(3)	2.617(2)	2.609(2)	2.627(2)	2.624(2)	2.634(4)
Na–O2 ×2	2.392(2)	2.391(1)	2.393(1)	2.396(3)	2.398(2)	2.402(2)	2.400(2)	2.403(2)	2.397(3)
Na–O3	2.588(2)	2.589(2)	2.586(2)	2.579(3)	2.572(2)	2.561(2)	2.560(2)	2.550(3)	2.537(5)
Na–O3′	2.543(2)	2.547(2)	2.548(2)	2.546(3)	2.535(2)	2.536(2)	2.538(2)	2.532(3)	2.533(5)
Na–O4 ×2	2.378(2)	2.375(1)	2.381(1)	2.386(3)	2.389(2)	2.395(2)	2.392(2)	2.394(2)	2.388(3)
Mean Na–O	2.481	2.482	2.485	2.489	2.489	2.489	2.492	2.491	2.489
Ti1–O1 ×2	2.049(1)	2.048(1)	2.043(1)	2.034(2)	2.025(1)	2.026(1)	2.022(1)	2.017(1)	2.013(2)
Ti1–O3	2.023(2)	2.024(1)	2.021(1)	2.010(2)	2.005(2)	2.002(2)	2.000(1)	1.988(2)	1.972(3)
Ti1–O4 ×2	2.051(1)	2.048(1)	2.041(1)	2.030(2)	2.016(1)	2.009(1)	2.005(1)	1.996(1)	1.987(2)
Ti1–O4′	1.932(2)	1.937(1)	1.942(1)	1.956(2)	1.957(2)	1.963(1)	1.968(1)	1.974(2)	1.988(3)
Mean Ti1–O	2.026	2.026	2.022	2.016	2.007	2.006	2.004	1.998	1.993
Ti2–O1	1.975(2)	1.977(2)	1.980(2)	1.981(3)	1.974(2)	1.973(2)	1.972(2)	1.975(2)	1.977(3)
Ti2–O2 ×2	2.012(1)	2.012(1)	2.008(1)	2.000(2)	1.989(1)	1.988(1)	1.985(1)	1.980(1)	1.982(2)
Ti2–O2′	2.020(2)	2.019(1)	2.022(2)	2.018(3)	2.026(2)	2.020(2)	2.021(1)	2.016(2)	2.007(3)
Ti2–O3 ×2	1.997(1)	1.995(1)	1.995(1)	1.995(2)	1.994(1)	1.993(1)	1.993(1)	1.995(1)	1.996(2)
Mean Ti2–O	2.002	2.002	2.001	1.998	1.994	1.993	1.992	1.990	1.989

[a]Data after Akimoto and Takei [4].

environments of the O atoms around the Ti1 and Ti2 atoms become more similar to each other (Fig. 5). In addition, the average octahedral Ti1–O and Ti2–O distances in the $Na_xTi_2O_4$ compounds decrease with x from 2.026 and 2.002 Å for $NaTi_2O_4$, to 1.993 and 1.989 Å for $Na_{0.558}Ti_2O_4$, respectively. The decrease in the Ti–O distances with the Na deficiency is in agreement with the fact that the formal Ti valence states increase from +3.5 in $NaTi_2O_4$ to +3.721 in $Na_{0.558}Ti_2O_4$.

The mixed-valence state of each Ti atom has been evaluated by bond valence analysis using the VALENCE program [17], as shown in Fig. 6. The mean valence state of $Na_xTi_2O_4$ gradually increases with the Na deficiency from 3.39 in $NaTi_2O_4$ to 3.64 in $Na_{0.558}Ti_2O_4$; moreover, these states are very consistent with the formal valence states estimated by the chemical formulae. On the other hand, a significant difference is observed between the Ti valence states of the Ti1 and Ti2 cations in the parent $NaTi_2O_4$ compound, the values of which are 3.26 and 3.51 for Ti1 and Ti2, respectively. Interestingly, the difference gradually decreases with the Na deficiency, and the valence states in $Na_{0.558}Ti_2O_4$ are 3.62 and 3.66 for Ti1 and Ti2, respectively. Furthermore, these valence changes show a discontinuity between $x = 0.751$ and 0.799, as observed in the lattice parameters (Fig. 3). Based on these facts, we speculate that the Ti1 sites are preferentially occupied by Ti^{3+} cations over the compositional range of $0.8 < x < 1$, while both the Ti1 and Ti2 sites are randomly occupied by Ti^{3+} and Ti^{4+} cations at $x = 0.558$. Accordingly, these data may suggest an order–disorder transition of the Ti^{3+} occupation at both the Ti sites together with the Na deficiency. This speculation shows good consistency with the results of the magnetic measurements; that is, correlated Ti^{3+}–Ti^{3+} spin couplings are observed only in $NaTi_2O_4$ and $Na_{0.912}Ti_2O_4$, as mentioned later. Furthermore, Geselbracht et al. [13] have suggested the partial charge segregation in $NaTi_2O_4$ as $NaTi1^{(3.5-\delta)+}Ti2^{(3.5+\delta)+}O_4$ based on the results of band calculations and transport measurements.

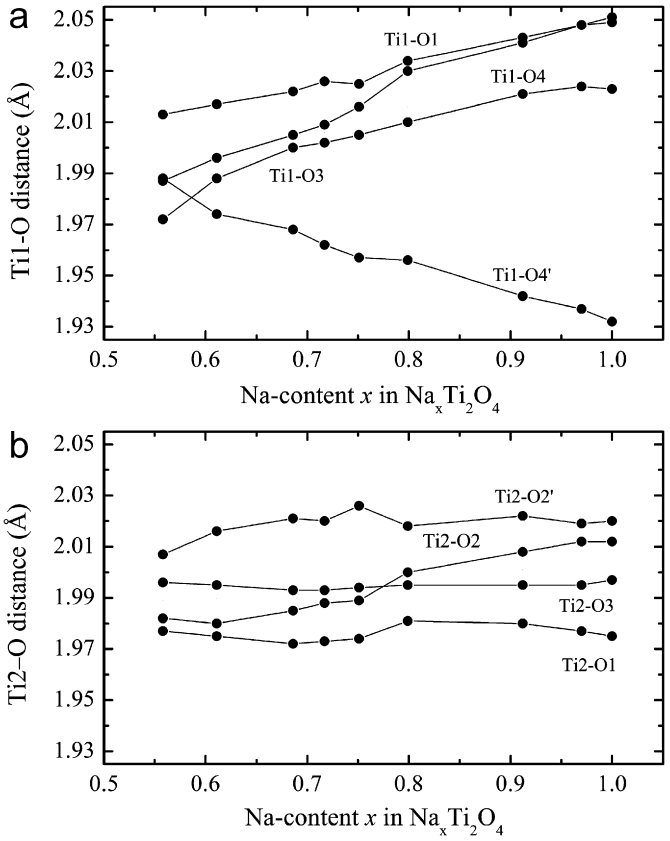

Fig. 5. Ti–O distances (Å) versus x in $Na_xTi_2O_4$ for (a) $Ti1O_6$ and (b) $Ti2O_6$ octahedra.

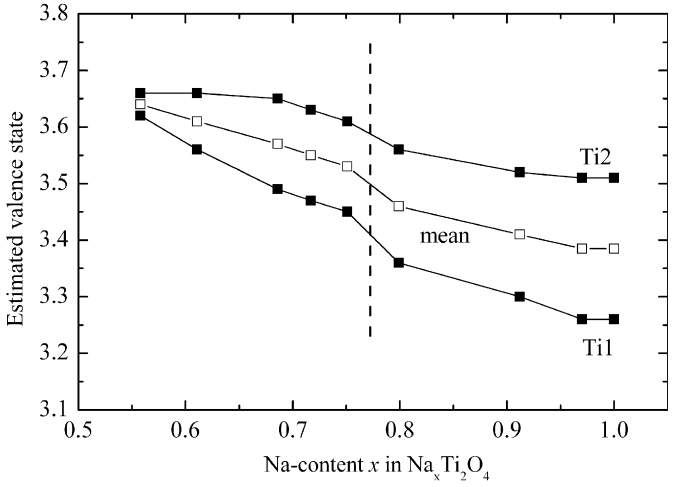

Fig. 6. Calculated valence state for the Ti atoms by bond valence analysis versus x in $Na_xTi_2O_4$.

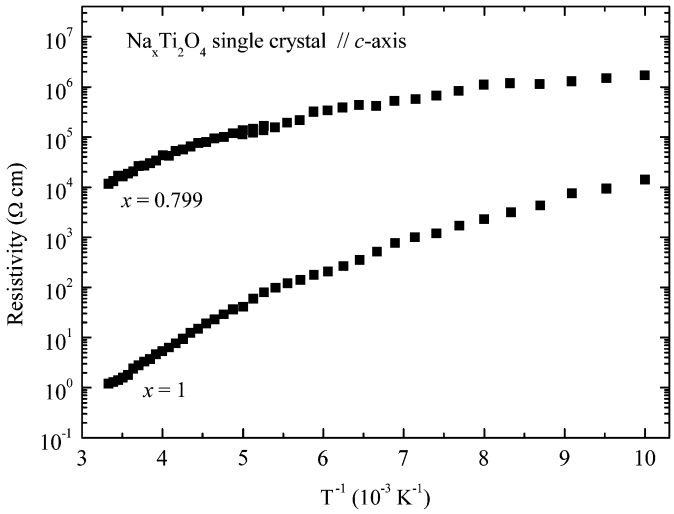

Fig. 7. Temperature dependence of the electrical resistivity of $Na_xTi_2O_4$ ($x = 1$ and 0.799) single crystals.

3.3. Physical properties

Fig. 7 shows the temperature dependence of electrical resistivity, measured along the needle (c-axis) direction, for single crystals of as-grown $NaTi_2O_4$ and Na-deficient $Na_{0.799}Ti_2O_4$. The resistivity of $NaTi_2O_4$ at 300 K is approximately 1.2 Ω cm, and a semiconducting behavior is observed below room temperature. The result shows good consistency with that of a recent study [13]. On the other hand, the resistivity of $Na_xTi_2O_4$ increases with the Na deficiency; however, $Na_xTi_2O_4$ is semiconductive in all the samples. The resistivity value of $Na_{0.799}Ti_2O_4$ is approximately 12 kΩ cm at 300 K, as shown in Fig. 7.

The Seebeck coefficient for the $Na_xTi_2O_4$ single crystals was measured at 300 K. The Seebeck coefficients for these compounds showed negative values, indicating n-type behavior. The value for $Na_{0.717}Ti_2O_4$ was $-67\,\mu V/K$ at 300 K, which was comparable to those reported for some reduced titanates, e.g., perovskite-type $Sr_{0.90}La_{0.10}TiO_3$ [3].

Fig. 8 shows the magnetic susceptibility χ of the three $Na_xTi_2O_4$ samples below 300 K. The χ value of as-grown $NaTi_2O_4$ showed a broad maximum around 40 K and decreased rapidly with the temperature, followed by an upturn below 10 K. The broad peak suggested the existence of short-range Ti^{3+}–Ti^{3+} spin correlations. The upturn below 10 K was considered to be due to the existence of isolated free Ti^{3+} ions or defects. From an inverse χ versus T plot below 10 K, the concentration of free spins with a Weiss temperature of −2.6(4) K was estimated to be 2.4% in $NaTi_2O_4$. A similar set of susceptibility data having a low-temperature tail and a broad maximum around 400 K was recently reported [13]. It was considered that a slight compositional difference between the present $NaTi_2O_4$ and the reported sample affected the temperatures of the broad maximums at 40 and 400 K, respectively. Note that the lattice parameters of the previous sample [12] are slightly smaller than those of the present $NaTi_2O_4$. This fact may suggest that the previously reported sample had an Na-deficient composition. Unfortunately, the analytical chemical composition of the sample has not been reported [12,13].

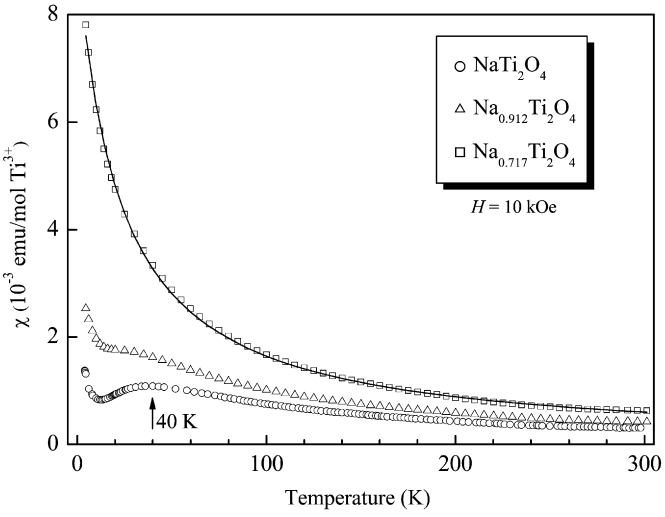

Fig. 8. Temperature dependence of the magnetic susceptibility of $Na_xTi_2O_4$ ($x = 1$,0.912 and 0.717) single crystals. The solid line represents a fit to the Curie–Weiss law.

On the other hand, the broad maximum around 40 K is suppressed by the Na deficiency in $Na_{0.912}Ti_2O_4$ and vanishes in the case of $Na_{0.717}Ti_2O_4$ (Fig. 8); this occurs because the increase in the number of diamagnetic Ti^{4+} cations in the chain induces a break in the correlated Ti^{3+}–Ti^{3+} spin coupling.

From the result of the bond valence analysis, we conclude that the Ti1 sites are preferentially occupied by the Ti^{3+} cations over the compositional range of $0.8 < x < 1$. Therefore, the Ti^{3+}–Ti^{3+} spin correlations observed in $NaTi_2O_4$ and $Na_{0.912}Ti_2O_4$ may occur preferentially in the Ti1 double chain. We attempted to fit the χ data of $NaTi_2O_4$ after subtracting the contribution of

isolated free Ti^{3+} ions using linear spin models; however, attempts to fit the magnetic data using the $S = 1/2$ uniform Heisenberg-chain model or the dimer model were unsuccessful. We think that the Ti–Ti distance along the chain direction is very important to control the Ti^{3+}–Ti^{3+} spin correlation. A similar feature of the Ti–Ti bonding has recently been reported using band calculations [13]. As the c-axis length directly corresponds to the Ti–Ti distance, the observed discontinuity of the lattice parameter around $x = 0.75$ may be caused by the magnetic correlation, although the difference in the c-axis lengths is very small. A further investigation should be performed to reveal the precise magnetic properties of the $Na_xTi_2O_4$ samples with $0.8 < x < 1$.

The χ data for $Na_{0.717}Ti_2O_4$ were fitted to the Curie–Weiss law over the temperature range from 4 to 300 K (Fig. 8). The extracted Curie constant (C) and the Weiss temperature (θ) are 0.206(3) K emu/mol-Ti^{3+} and −22.5(4) K, respectively. A plot of χ^{-1} as a function of temperature is nearly linear between 4 and 300 K, confirming the validity of the above relation. From the obtained C value, the effective magnetic moment in $Na_{0.717}Ti_2O_4$ is determined to be $\mu_{eff} = 1.28\,\mu_B$, which is considerably smaller than the expected value of $1.73\,\mu_B$ for the free Ti^{3+} spins of $S = 1/2$ and $g = 2$. This fact may indicate that the correlated Ti^{3+}–Ti^{3+} spin interaction did not completely disappear even in $Na_{0.717}Ti_2O_4$.

4. Conclusion

Single crystals of $NaTi_2O_4$ having millimeter-sized needle shapes were synthesized by a reaction of Na metal and TiO_2 in a sealed iron vessel at 1473 K. Sodium-deficient $Na_xTi_2O_4$ single crystals with $0.558 < x < 1$ were successfully prepared by a topotactic chemical oxidation method at room temperature. The crystal structures of $Na_xTi_2O_4$ having different Na contents were determined by the single-crystal X-ray diffraction method. The electrical resistivity, Seebeck coefficient, and magnetic susceptibility data of the $Na_xTi_2O_4$ single-crystal samples have been measured for the first time. The compositional discontinuity in the structural and magnetic properties around $x = 0.8$ can be explained by an order–disorder transition of the Ti^{3+} occupation at two Ti sites occurring simultaneously with the Na deficiency.

Acknowledgment

The authors are greatly indebted to Prof. Humihiko Takei for fruitful discussions on the single-crystal growth and physical properties of $NaTi_2O_4$.

Appendix A. Supplementary Materials

Supplementary data associated with this article can be found in the online version at doi:10.1016/j.jssc.2006.12.023.

References

[1] D.C. Johnston, J. Low Temp. Phys. 25 (1976) 145–175.
[2] T. Ohzuku, A. Ueda, N. Yamamoto, J. Electrochem. Soc. 142 (1995) 1431–1435.
[3] T. Okuda, K. Nakanishi, S. Miyasaka, Y. Tokura, Phys. Rev. B 63 (2001) 113104.
[4] J. Akimoto, H. Takei, J. Solid State Chem. 79 (1989) 212–217.
[5] J. Akimoto, Y. Gotoh, K. Kawaguchi, Y. Oosawa, J. Solid State Chem. 96 (1992) 446–450.
[6] J. Akimoto, Y. Gotoh, M. Sohma, K. Kawaguchi, Y. Oosawa, H. Takei, J. Solid State Chem. 110 (1994) 150–155.
[7] J. Akimoto, Y. Gotoh, Y. Oosawa, N. Nonose, T. Kumagai, K. Aoki, H. Takei, J. Solid State Chem. 113 (1994) 27–36.
[8] R.K.B. Gover, J.R. Tolchard, H. Tukamoto, T. Murai, J.T.S. Irvine, J. Electrochem. Soc. 146 (1999) 4348–4353.
[9] A. Kuhn, R. Amandi, F. Garcia-Alvarado, J. Power Sour. 92 (2001) 221–227.
[10] L. Brohan, R. Marchand, M. Tournoux, J. Solid State Chem. 72 (1988) 145–153.
[11] J. Akimoto, H. Takei, J. Solid State Chem. 85 (1990) 31–37.
[12] M.J. Geselbracht, L.D. Noailles, L.T. Ngo, J.H. Pikul, R.I. Walton, E.S. Cowell, F. Millange, D. O'Hare, Chem. Mater. 16 (2004) 1153–1159.
[13] M.J. Geselbracht, A.S. Erickson, M.P. Rogge, J.E. Greedan, R.I. Walton, M.W. Stoltzfus, H.W. Eng, P.M. Woodward, J. Solid State Chem. 179 (2006) 3489–3499.
[14] M. Latroche, L. Brohan, R. Marchand, M. Tournoux, J. Solid State Chem. 81 (1989) 78–82.
[15] S.R. Hall, D.J. du Boulay, R. Olthof-Hazekamp (Eds.), Xtal3.5 System, University of Western Australia, Australia, 2000.
[16] R.D. Shannon, Acta Crystallogr. A 32 (1976) 751–767.
[17] I.D. Brown, J. Appl. Crystallogr. 29 (1996) 479–480.